Ab Initio Molecular Dynamics of Liquid 1,3-Dimethylimidazolium Chloride

Michael Bühl,*,† Alain Chaumont,‡ Rachel Schurhammer,‡ and Georges Wipff*,‡

Max-Planck-Institut für Kohlenforschung, Kaiser-Wilhelm-Platz 1, D-45470 Mülheim an der Ruhr, Germany, and Laboratoire MSM, UMR 7551 CNRS, Institut de Chimie, 4 rue Blaise Pascal, F-67000 Strasbourg, France

Received: April 8, 2005; In Final Form: June 21, 2005

Density-functional-based Car−Parrinello molecular dynamics (CPMD) simulations have been performed for the ionic liquid 1,3-dimethylimidazolium chloride, [dmim]Cl, at 438 K. The local structure of the liquid is described in terms of various partial radial distribution functions and anisotropic spatial distributions, which reveal a significant extent of hydrogen bonding. The cation−anion distribution simulated with the BP86 functional is in qualitative agreement with the structural model derived from neutron diffraction data for the liquid, whereas the theoretical cation−cation distribution shows less satisfactory accord. Population analyses indicate noticeable charge transfer from anions to cations, and specific CH···Cl hydrogen bonds are characterized in terms of donor−acceptor interactions between lone pairs on Cl and antibonding σ^*_{CH} orbitals.

Introduction

What makes ionic liquids so special that their design and use has evolved into a blossoming branch of chemistry? Their attractive macroscopic properties are well-known, such as nonvolatility, noninflammability, excellent solvating capabilities, and many more.[1] By choosing appropriate constituent cations and anions, these properties can be finely tuned and tailored, which has led to a surge of applications in chemistry.[2,3] On a microscopic, molecular level, however, knowledge of the factors that determine these properties remains fragmentary.

For the particularly important class of imidazolium-based ionic liquids, extensive hydrogen-bonding networks are observed in the solid state,[4,5] which are believed to be preserved to a large extent in the liquid.[6] In recent ab initio studies attempts have been made to relate such specific cation−anion interactions with macroscopic properties.[7,8] These computations were performed for single, static ion pairs. To address the dynamic aspects of such interactions in the whole ensemble, and to elucidate and predict the structures of ionic liquids, molecular dynamics (MD) simulations are being carried out at an increasing rate.[9] These simulations can afford quite detailed insights into the dynamic nature of these solvents, and can be used to investigate the microscopic roots of their properties, for instance in liquid−liquid extractions.[10] To date, virtually all of these MD simulations are performed using classical, molecular-mechanical force fields.[11,12] Results and predictive power of such calculations can depend critically on the particular force-field parameters.[13] For a critical assessment of the performance of classical force fields for ionic liquids, direct comparison to accurate quantum-chemical MD data would be desirable. We now present such a study using the popular Car−Parrinello approach (CPMD),[14] which performs very well in the description of polar molecular liquids such as water and solutions therein.[15]

As a target system we chose 1,3-dimethylimidazolium chloride, [dmim]Cl (Chart 1), one of the simplest imidazolium-based ionic liquids. Even though, due to its more elevated melting point, [dmim]Cl is not a member of the family of room temperature ionic liquids, it can be considered as a prototypical model for the latter. A neutron-diffraction study of molten [dmim]Cl has been presented recently,[16] calling special attention to the mutual distribution and ordering of cations and anions, as assessed by suitable spatial and partial radial distribution functions. Since the refinement of the experimental data has involved Monte Carlo simulations using classical, empirical potentials,[17] the comparison with the independent, parameter-free CMPD results is of interest in its own right.

CHART 1

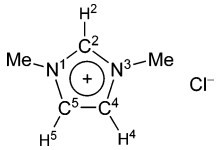

This paper is organized as follows: After a brief summary of the theoretical methods, derivation and setup of the computational model is described in detail, followed by a discussion of the actual MD results. During write-up of this paper, a related DFT-based MD study by Del Pópolo et al. of the same system appeared,[12] which we will refer to at the appropriate places in the discussion.

Computational Details

Geometries of isolated monomeric ion pairs have been fully optimized using 6-31+G** basis[18] together with the correlated ab initio MP2 method and a number of gradient-corrected and hybrid density functional combinations denoted as BP86,[19,20] BLYP,[19,21] PBE,[22] and B3LYP.[23,21] For the DFT methods, the nature of each stationary point was verified by analytic calculation of the harmonic vibrational frequencies. These computations were carried out with the Gaussian 98 program package[24] (Gaussian 03[25] for PBE).

For the bulk liquid, Car−Parrinello MD simulations were performed with the CPMD program,[26] employing the BP86 functional combination, together with norm-conserving pseudopotentials generated according to the Troullier and Martins procedure[27] and transformed into the Kleinman−Bylander

† Max-Planck-Institut für Kohlenforschung. Fax: +(0) 208-306 2996. E-mail: buehl@mpi-muelheim.mpg.de.
‡ Laboratoire MSM. E-mail: wipff@chimie.u-strasbg.fr.

10.1021/jp0518299 CCC: $30.25
Published on Web 09/13/2005

form.[28] Periodic boundary conditions were imposed using cubic supercells with 25 and 41 ion pairs with box lengths of 16.96 and 20.00 Å, respectively, and starting configurations obtained from AMBER simulations (vide infra). Kohn−Sham orbitals were expanded in plane waves up to a kinetic energy cutoff of 60 Ry. Unconstrained simulations (NVE ensemble) were performed using a fictitious electronic mass of 600 au and a time step of 0.121 fs. To keep this time step, hydrogen was substituted with deuterium. The systems were equilibrated for 0.5 ps maintaining a temperature of 425(±50) K via velocity rescaling, and were then propagated without constraints, affording final averaged temperatures of ca. 438(13) and 450(9) K for the smaller and the larger box, respectively (standard deviation during the last picosecond in parentheses).

Atomic charges were obtained from Mulliken (MPA) and Natural Population Analysis (NPA),[29] as well as from schemes based on the fitting to the electrostatic potential (denoted ESP[30] and ChelpG[31]). Wave functions from CPMD snapshots were fully converged for this purpose, and the orbitals represented in plane waves were projected onto suitable atomic orbitals.[32] The converged wave functions were also used to construct maximally localized orbitals (Wannier functions).[33]

Classical MD simulations were performed with the AMBER7.0 software,[34] based on the empirical representation of the potential energy U:

$$U = \sum_{\text{bonds}} k_b(b - b_0)^2 + \sum_{\text{angles}} k_\theta(\theta - \theta_0)^2 + \sum_{\text{dihedrals}} \sum_n V_n(1 + \cos(n\varphi - \gamma)) + \sum_{i<j} \left[\frac{q_i q_j}{R_{ij}} - 2\epsilon_{ij}\left(\frac{R^*_{ij}}{R_{ij}}\right)^6 + \epsilon_{ij}\left(\frac{R^*_{ij}}{R_{ij}}\right)^{12} \right]$$

The corresponding atomic charges are given in Table S1. The Cl parameters ($R^* = 2.107$ Å, $\epsilon = 0.1639$ kcal/mol) are the same as in the $AlCl_4^-$ anion of ref 35. Eight models of the $dmim^+$ cation have been considered: The parameters of model 1 have been adapted from those of the butylmethylimidazolium ion.[35] In model 2, the $dmim^+$ and Cl^- charges have been scaled by 0.9, to mimic the anion-to-cation charge transfer of 0.1e, as calculated by QM calculations.[36] In model 3 and model 4 we have employed the $dmim^+$ charges and parameters from ref 37 and 13, respectively. Model 5 uses the charges derived from the MPA analysis of the CPMD trajectory (vide infra). In all these models, the aromatic C^2-H, C^4-H, and C^5-H protons are weakly polar. This is why model 6 to model 8 were constructed with an increased $C^{\delta-}-H^{\delta+}$ polarity (see Table S1). The nonbonded electrostatic interactions were calculated with the Ewald method. The MD simulations were performed at 425 K, starting with random velocities and a time step of 1 fs. Three cubic solvent boxes (box 1 to box 3), of 17, 20, and 38.2 Å side, respectively, were prepared, starting from the X-ray structure of [dmim]Cl.[4] They contained 25, 41, and 300 $dmim^+$ Cl^- ion pairs, respectively. Their characteristics and simulation conditions are given in Table S2. The small box 1 and box 2 systems were simulated with model 1 and a cutoff of 6 Å for 1-6-12 interactions, whereas for the large box 3 we compared all eight models 1 to 8, using a cutoff of 12 Å. After 1000 steps of energy minimization, we performed 500 ps of dynamics at constant volume, followed by 1 ns at a constant pressure of 1 atm. The production step consisted of 2 ns at constant volume.

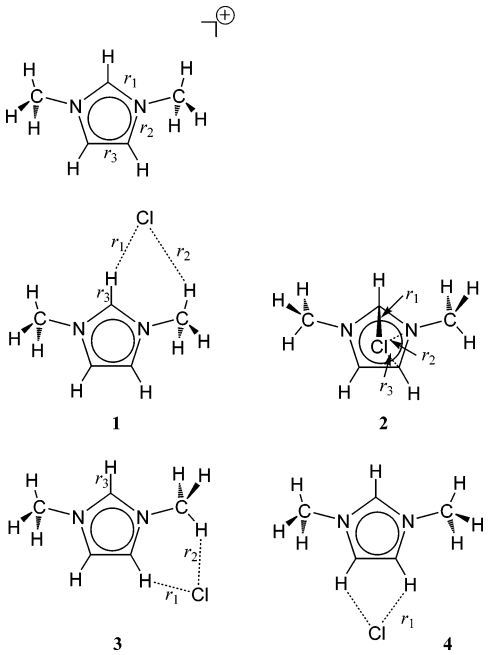

Figure 1. Labeling of $dmim^+$ and [dmim]Cl isomers.

TABLE 1: Selected Geometrical Parameters and Relative Energies of $dmim^+$ and [dmim]Cl Stationary Points 1−4 (6-31+G Basis, Isolated Ion or Ion Pairs in the Gas Phase)**

molecule	parameter[a]	MP2	BP86	BLYP	PBE	B3LYP
dmim$^+$	r_1	1.344	1.350	1.353	1.347	1.339
	r_2	1.376	1.389	1.394	1.386	1.383
	r_3	1.374	1.375	1.376	1.373	1.364
1	r_1	2.006	1.925	1.977	1.919	1.990
	r_2	2.565	2.563	2.642	2.573	2.620
	r_3	1.111	1.152	1.139	1.152	1.125
	(E_{rel})	(0.0)	(0.0)	(0.0)	(0.0)	(0.0)
2	r_1	2.697	2.530	2.646	2.518	2.662
	r_2	3.132	3.151	3.240	3.140	3.225
	r_3	3.634	3.837	3.959	3.825	3.902
	(E_{rel})	(−1.2)	(0.5)	(0.7)	(0.2)	(1.1)
3	r_1	2.152	2.076	2.132	2.076	2.149
	r_2	2.355	2.308	2.365	2.305	2.353
	r_3	1.076	1.087	1.085	1.087	1.079
	(E_{rel})	(7.5)	(7.8)	(7.7)[b]	(7.9)[b]	(8.1)
4	r_1	2.525	2.497	2.557	2.496	2.547
	(E_{rel})	(13.6)	(15.2)	(14.3)[c]	(15.3)	(14.7)

[a] Distances r in Å (see Figure 1 for definition), energies relative to **1** in kcal/mol. [b] Transition state for Me rotation. [c] Transition state for Cl migration.

Results and Discussion

Construction of the Model for CPMD Simulations. In practice, the use of CPMD is restricted to local (LDA) and gradient-corrected, nonhybrid density functionals. To validate the latter concerning their description of hydrogen bonding between $dmim^+$ cations and Cl^- anions, several isomers of an isolated [dmim]Cl cluster have been optimized, in which the anion is attached to different locations around the imidazolium core (**1**−**4**, Figure 1). Results obtained with BP86, BLYP, PBE, and B3LYP functionals are summarized in Table 1, together with the corresponding MP2 data (all using 6-31+G** basis) as reference.

Overall, the DFT results reproduce the MP2 data quite well, with one notable exception: the energetic sequence between the two lowest minima **1** and **2** is reversed between MP2 and DFT. The former predicts a slight preference for the face-coordinated form **2**, probably favored by attractive dispersion

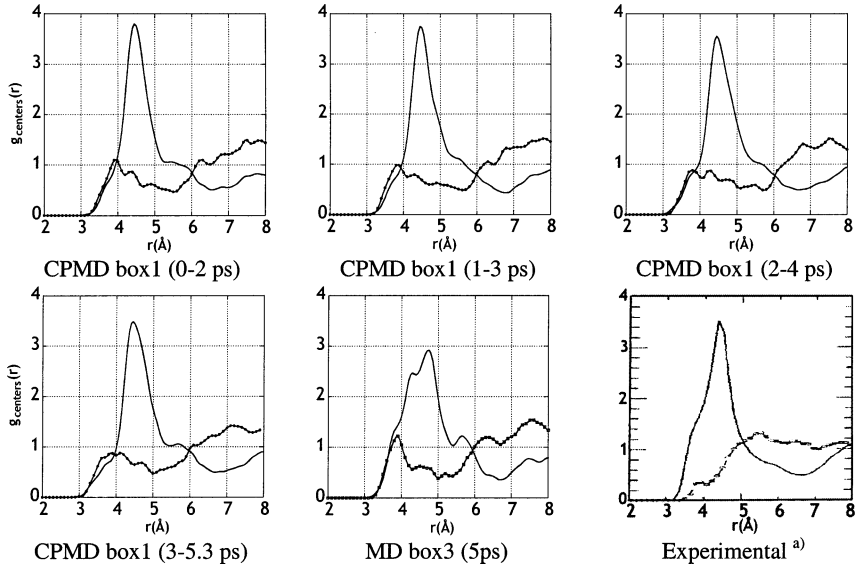

Figure 2. Radial distribution functions for the cation−cation (circle + line) and cation−anion (line) distribution extracted from the simulations of the smaller box. (superscript a) Experimental: section of the rdfs derived in ref 16 (reprinted with permission. Copyright 2003, American Institute of Physics).

forces absent in the DFT methods. A polar medium, however, should stabilize **1** with its larger dipole moment, and in fact, when immersed in a polarizable continuum, **1** is lower in energy than **2** also at the MP2 level.[38] DFT methods should thus offer a faithful description of the cation−anion interactions in the bulk liquid phase.

Among themselves the DFT variants employed yield very similar results, and there appears to be little reason to favor one functional over the other. In particular, judging from the data in Table 1, the pure gradient-corrected functionals, BP86, BLYP, and PBE, perform as well as the B3LYP hybrid variant. Eventually, we chose BP86 for the CPMD simulations, because some of the higher lying stationary points were not true minima with BLYP and PBE. In their DFT-MD study,[12] Del Pópolo et al. used the PBE functional, which should thus give quite comparable results to our BP86 data.[39]

Geometry optimizations of a single $dmim^+$ ion with the CPMD program (in a large box with a cell parameter of 17 Å) and numerical computation of harmonic frequencies were performed with several values for the energy cutoff, and the results were sufficiently converged and entirely compatible with the BP86/6-31+G** data with a cutoff of 60 Ry. The same was found for the relative energies and optimized geometrical parameters of isolated **1** and **2** (bond distances and relative energies within ca. 0.02 Å and 0.6 kcal/mol, respectively, of the nonperiodic BP86/6-31+G** results).

For the simulation of the bulk, two cubic boxes containing 25 and 41 [dmim]Cl units were generated with cell parameter chosen as to render the experimental density of 1.1233.[40] Starting structures were taken from corresponding classical MD runs equilibrated for 500 ps at 425 K, and CPMD simulations were performed using the parameters described in the Computational Details section above. Simulations for the smaller and larger boxes were continued for a total of 5.3 and 2.3 ps, respectively. Even for a massively parallel supercomputer, these are demanding calculations requiring, for the larger box, ca. 160 h per picosecond on 128 CPUs.

Structure and Dynamics. First we will discuss results from the simulation of the smaller box. The course of the simulation is monitored in terms of suitable radial distribution functions (rdfs), also called pair correlation functions $g(r)$,[41] involving the centers of each imidazole ring (Im) and the Cl^- ions. The Im-Im and Im-Cl rdfs are computed over overlapping windows of 2 ps (first four pictures in Figure 2) to gauge the time evolution of the bulk structure and its eventual convergence.

It turns out that the $g_{ImIm}(r)$ curve (solid line with dots in Figure 2) is not stationary during the time frame considered. At the beginning of the simulation there is a notable maximum at r just below 4 Å (with $g(r)$ slightly larger than 1, cf. first frame in Figure 2). As the simulation proceeds, this peak gradually decreases in intensity, whereas features between 4 and 6 Å become apparent or more prominent. These features are probably artifacts of the limited sampling time, 2 ps per window, in conjunction with the very low mobility (rate of diffusion) of the bulky cations relative to each other. Apparently, much longer simulation times would be necessary for a fully equilibrated cation distribution. The computed Im-Im rdf at the end of the 5.2 ps simulation is not in good agreement with the one derived from the experimental data (last picture in Figure 2). The latter has only a small shoulder just below 4 Å and a shallow maximum between 5 and 6 Å, and has all but decayed to the statistical value of 1 beyond that. In contrast, the theoretical $g_{ImIm}(r)$ curves have a pronounced maximum between 7 and 8 Å, and do not approach 1 at the latter value (which marks half of the box length). Clearly, the box size is too small, which may add to the artifacts introduced by the limited simulation time (see below for results from a larger box). The pronounced maximum in $g_{ImIm}(r)$ at r below 4 Å is not apparent in the DFT-based MD simulations of ref 12; in our simulations it reflects the cation distribution from the starting configuration, generated from an AMBER simulation. Possibly, that particular force field tends to favor somewhat shorter cation−cation separations, as it shows a certain propensity for π stacking of the Im moieties.[42]

The $g_{ImCl}(r)$ curve, on the other hand (solid line in Figure 2), shows only little variations with time and is in good qualitative accord with the result derived from experiment. In all these rdfs, the main peak is centered at ca. 4.5 Å, with an intensity of $g(r) \approx 3.5$, and is flanked by two shoulders at shorter and longer distances (ca. 3.7 and 5.5 Å, respectively). The chloride anions are smaller and more mobile than the $dmim^+$ moieties, which, apparently, facilitates equilibration of the anion distribution around the more sluggish cations.

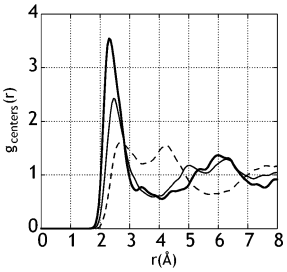

Figure 3. Individual $g_{HCl}(r)$ pair correlation functions involving H^2 (bold line), $H^{4,5}$ (solid), and H(Me) (dashed); results from CPMD box 1.

As the dynamics of ionic liquids is characterized by "rattle" motions of ions in long-lived cages, with quite long relaxation times for orientation motions (in the order of 200 ps in the case of 1-ethyl-3-methylimidazolium nitrate[9b]), our CPMD trajectories cannot be considered as equilibrated with respect to the quantum Hamiltonian and are still reminiscent of the starting AMBER configuration. However, a significant relaxation and repositioning of anions with respect to the cations occurs in the CPMD simulations, consistent with the fact that fast subpicosecond dynamics, mainly due to the anion contributions, are responsible for more than 50% of the entire relaxation of solvent fluctuations in the studied liquid.[43]

During the approximately 5 ps of the total simulation, the distribution of the chloride anions around the $dmim^+$ cations is largely governed by hydrogen bonding, as revealed by the $g_{HCl}(r)$ pair correlation functions displayed in Figure 3. In particular, the pronounced maximum in the rdf involving H^2, $g_{HCl}(r) \approx 3.5$ at $r \approx 2.3$ Å (bold line in Figure 3), betrays a strong preference of chloride for this binding site. The same is apparent from the mean numbers of Cl ions around each type of H atom, obtained by integration over the individual $g_{HCl}(r)$ curves up to 3.2 Å, which are 1.0, 0.82, and 0.7 per H^2, $H^{4,5}$, and H(Me) atom, respectively (note that these include the statistical weighting factors of 1, 2, and 6, respectively). Qualitatively similar results have been reported from the PBE MD simulations in ref 12.

Average coordination numbers obtained from the rdfs hide, however, a broad diversity of situations, which are revealed by visual inspection of the trajectories and by the analysis of $H_{ar}\cdots Cl$ contacts in solution, as compared to the solid state. In the crystal,[4] each Cl^- anion is pinched between two coplanar $dmim^+$ cations (see Figure S1 of the Supporting Information), forming hydrogen bonds with the C^2-H^2 proton of one cation and the C^4-H^4 proton of the other cation (at 2.6 Å), complemented by adjacent methyl protons. In solution, more diverse environments of the $C_{ar}-H$ protons around Cl^- can be found, as monitored, for instance, by the number of $C_{ar}H\cdots Cl$ contacts during the dynamics. Using a purely geometrical selection criterion (namely a $H\cdots Cl$ distance shorter than 3.0 Å), the number of such contacts can vary between 0 and 5. The evolution of this number for all Cl^- ions as a function of time is illustrated in Figure S2. Let us consider two typical examples from the ensemble (Cl-405 and Cl-425 anions in Figure S2). In one case (Cl-405) the first shell does not comprise C^2-H^2, but three $C^{4,5}-H^{4,5}$ protons belonging to three different $dmim^+$ moieties, on average at 2.67 ± 0.14, 2.66 ± 0.35, and 3.71 ± 1.3 Å, respectively, during 5 ps. The first two distances are comparable to those in the crystal, whereas the latter is longer (actually, it is formed only after 2 ps of simulation, see Figure S3a). In another case (Cl-425) the environment differs and comprises three C^2-H^2 plus one C^4-H^4 protons (at 3.4 ± 0.61, 2.50 ± 0.26, 2.71 ± 0.45, and 3.60 ± 0.87 Å, respectively, on average). There are thus two short hydrogen bonds as in the crystal, and longer ones (see also the cumulated views of these two environments in Figure 4 below). During the dynamics, the number of aromatic protons at less than 3 Å from Cl^- oscillates between 2 and 5 for Cl-425 and between 1 and 4 for Cl-405, leading to average "coordination numbers" of 3.2 ± 0.8 and 2.0 ± 0.6 $C_{ar}-H$ protons, respectively. In all cases, there is a more versatile coordination of the methyl protons, which are less acidic and more mobile than the aromatic protons. For the other Cl^- anions, various time dependent combinations of the $C_{ar}-H$ protons occur during the dynamics, as illustrated in Figure S2.

Generally, the shortest $C-H\cdots Cl$ contacts correspond to more linear $C-H\cdots Cl$ bonds and to in-plane coordination of Cl^-, as seen, e.g., around Cl-425 (Figure S3). The $C-H\cdots Cl$ angle is ≈150 ± 20° for the H_{213}, H_{230}, and H_{302} protons which are at less than 2.7 Å, and 90 ± 20° for the more remote H_{185} proton at 3.4 ± 0.5 Å. The dynamic pictures that emerge from the CPMD simulations are thus quite different from those observed in the solid state or in the $dmim^+$ Cl^- ion pair. In no case, however, is Cl^- sandwiched between two $dmim^+$ rings, in keeping with the directionality of $C_{ar}H\cdots Cl$ hydrogen bonds with aromatic protons (vide infra).

Dynamics is also apparent from the trajectories of the Cl^- ions and their environment (see Figures 4 and 5). The root-mean-square fluctuations of the positions of Cl-405 and Cl-425 are 1.07 and 0.84 Å, respectively, i.e., similar to those of the surrounding $C_{ar}-H$ atoms (from 0.7 to 1.3 Å), indicating that Cl^- anions are moving inside a mobile "cage" of $dmim^+$ cations, as also illustrated by a cumulated view of their positions (see Figure 5). The corresponding averaged root-mean squares for *all* Cl^- anions (1.04 Å) and all $C_{ar}-H$ protons are comparable (1.08 Å). As expected, these root-mean-square fluctuations are fairly small and no real diffusion occurs, as this is known to happen on a much longer time scale.[9d] However, the dynamics of the Cl^- anions in their local basins should be well captured in the CPMD simulations.

The pair correlation functions discussed above only describe isotropic radial distributions, neglecting spatial anisotropies. Spatial density functions from classical and DFT-based MD simulations have revealed a noticeable preference for the location of the chloride anions along the CH bond vectors[12,13,16] and, in that function derived from the neutron-diffraction data,[16] to some extent also on top of the imidazole face. The corresponding density of Cl^- around the $dmim^+$ cations in the CPMD trajectory is illustrated in Figure 6, an overlay of all chloride positions about each of the 25 cations in the box (the latter have been centered and rotated to the same orientation, and snapshots have been taken every 27 fs during the last 2.5 ps of the simulation). The increased "concentration" of anions along the C^2-H^2 and $C^{4,5}-H^{4,5}$ axes is clearly visible as "clusters" of points in the upper center and lower corners, respectively, of the plot. To a lesser extent, there is also an increased probability of finding Cl^- near the methyl groups (not well visible from the 2D representation in Figure 6), fully consistent with the rdfs in Figure 3.

Selecting the Cl^- anions within a range of 3.5 Å from $C_{ar}-H$ protons during CPMD leads to a distribution of $C-H\cdots Cl$ angles with pronounced maxima at ≈150° for the C^2-H^2 and $C^{4,5}-H^{4,5}$ protons (see the upper part of Figure 7), thus confirming the stereochemistry of Cl^- coordination to the $dmim^+$ cations. The lack of such a peak in the AMBER results on the same box and time scale (model 1, see the lower part of Figure 7)

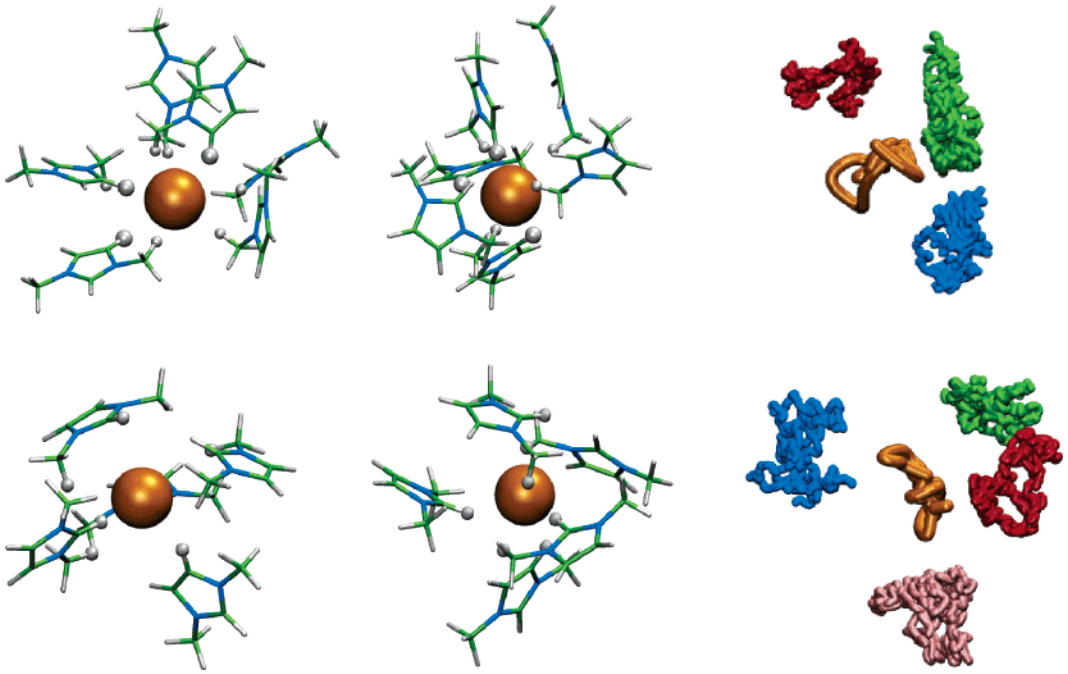

Figure 4. Orthogonal (left and middle) and cumulated views (right) of the environment of two representative Cl^- ions, no. 405 (top) and no. 425 (bottom). Cumulated views have been collected during the last 2.5 ps of dynamics of the H_{ar} bonded to Cl^-.

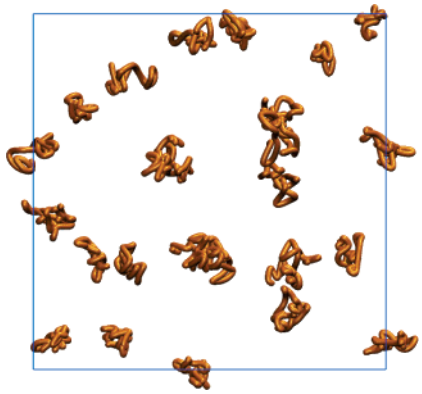

Figure 5. Cumulated views of the Cl^- positions in box 1 during the last 2.5 ps of CPMD dynamics.

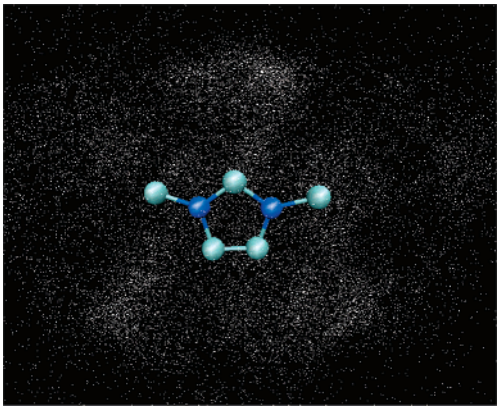

Figure 6. Density of Cl^- ions around the $dmim^+$ moieties, as obtained from the last 2.5 ps of the CPMD trajectory (overlay from all 25 cations in the smaller box). Hydrogens are omitted for clarity.

hints at the importance of polarization or stereoelectronic effects,[44] which are also revealed by the bonding analysis (vide infra).

The pronounced maxima in the AMBER distributions below 90° are partly related to the intermediate occurrence of "π-

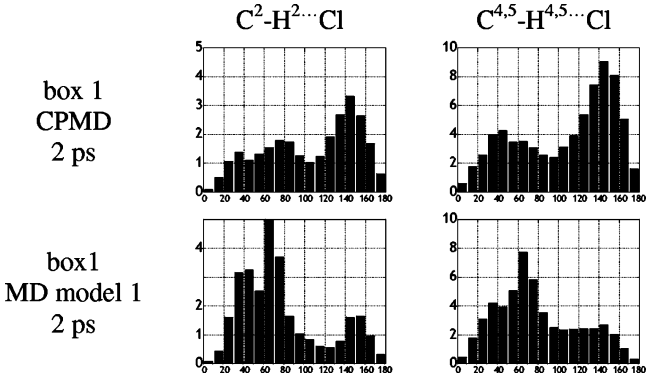

Figure 7. Statistical analysis of the C_{ar}−H···Cl angles for Cl atoms within 3.5 Å of aromatic protons. Curves obtained with other AMBER models are given in Supporting Information Figure S5.

stacked" arrangements as in **2**. In the CPMD trajectory, such arrangements occur much less frequently, and in the "Cl^- density" plotted in Figure 6, no enhanced density is noticeable on top of the imidazole face. That such cation−anion "π-stacking" interactions are not more prominent in the CPMD simulations may be related to the slight underestimation of the stability of such structures intrinsic to DFT (cf. the relative sequence of **1** vs **2** discussed above). Except from this detail, the cation−anion distribution emerging from the CPMD simulation is qualitatively similar to that derived from previous experimental, classical, and DFT-based MD studies, and reflects the importance of C−H···Cl interactions, in particular (as apparent from Figure 3) that involving H^2.

Bonding Analysis. At this point, the origin of this C^2−H^2···Cl binding preference deserves some scrutiny. Hydrogen bonds are among the principal forces that govern structure and properties of condensed phases, and their strength and nature emerges as a complex interplay between electrostatic, covalent, and dispersion contributions.[45] In a simple charge model, one would expect this particular H atom, H^2, to be more positively charged than the other ones because of the close proximity of two electronegative N atoms. As a consequence,

TABLE 2: Atomic Charges for Isolated 1, Computed at the BP86 Level Using Various Definitions,[a] Together with Ensemble Average for the Bulk from CPMD Simulation in the Smaller Box

atom[b]	ESP Gaussian	ESP CP-opt	ChelpG Gaussian	NPA Gaussian	MPA Gaussian	MPA CP-opt	MPA CPMD[c]
Cl	−0.73	−0.73	−0.73	−0.78	−0.67	−0.73	−0.75(3)
H^2	0.09	0.15	0.15	0.28	0.15	0.30	0.32(2)
$H^{4,5}$	0.22	0.19	0.18	0.27	0.18	0.31	0.30(2)
H(Me)	0.15	0.11	0.08	0.27	0.20	0.29	0.27(2)
C^2	0.03	−0.10	−0.03	0.24	−0.20	0.22	0.18(3)
$C^{4,5}$	−0.25	−0.22	−0.17	−0.09	−0.11	−0.07	−0.06(2)
C(Me)	−0.31	−0.21	−0.05	−0.52	−0.24	−0.48	−0.46(2)
N	0.20	0.24	0.13	−0.36	−0.06	−0.22	−0.20(1)

[a] See Computational Details; Gaussian denotes Gaussian 6-31+G** basis, CP-opt obtained for isolated **1** optimized with the CPMD program employing the same setup as for the MD simulations. [b] Averaged values, where appropriate. [c] Averaged over 20 snapshots between 3.0 and 5.0 ps; standard deviations are given in parentheses.

the Coulomb attraction to the anion should be strongest for this site. Essentially all population analyses, however, afford only marginal differences between the charge densities assigned to the individual imidazolium protons, either in **1** (see Table 2), or in pristine $dmim^+$ (not shown). Inspection of the electronic wave functions, on the other hand, provides evidence for direct binding interactions. These are apparent, for instance, from the shape of suitable localized orbitals, where the lone pairs on chloride, as described by maximally localized Wannier functions, are especially instructive. The lone pair directed toward H^2 in pristine **1** is illustrated in the top of Figure 8 (obtained from the BP86/CP-opt wave function). The strong polarization of the large sp^3 lobe toward the CH bond is clearly visible, as is, more importantly, a small contribution from the antibonding σ^*_{CH} orbital. The same is found in the BP86/6-31+G** wave function of isolated **1** after Boys localization of the canonical MOs (not shown).

This bonding interaction is also apparent in a Natural Bond Orbital (NBO)[29] analysis at the BP86/6-31+G** level: Second-order perturbational analysis reveals a strong donor−acceptor interaction from the lone pair NBO on Cl into the antibonding σ^*_{CH} NBO, the Natural Localized Cl lone pair (NLMO)—like the corresponding Wannier function—shows a pronounced delocalization tail on the adjacent CH group (ca. 8% contribution from this moiety), and the Wiberg Bond Index (WBI)[46] between Cl and H^2—which can be taken as an indicator for the covalent character of a bond—has a substantial value of 0.12. At the same time, the WBI between C^2 and H^2, 0.71, is significantly reduced with respect to that of the uncoordinated $C^{4,5}$−$H^{4,5}$ bonds, where it is 0.90. The presence and importance of such orbital interactions has been noted in other H-bonded systems before.[47]

To what extent is this donor−acceptor interaction preserved in the bulk liquid? Chloride ions in the vicinity of corresponding CH units, i.e., those that contribute to the largest peak in Figure 3, show indeed Wannier functions with the same characteristics as that of the minimized ion pair, namely polarization toward the hydrogen and small antibonding contribution at the CH unit. A typical snapshot is plotted in the middle and, enlarged, on the bottom of Figure 8. Clearly, such orbital interactions are not only present in tight, static ion pairs, but also in the dynamic ensemble.

In context with this donor−acceptor interaction, the extent of concomitant charge transfer between anions and cations is an important issue, as this can have consequences for the microstructure of ionic liquids inasmuch as this structure is governed by Coulomb forces. During refinement of parameters for classical force fields, the assignment of atomic charges

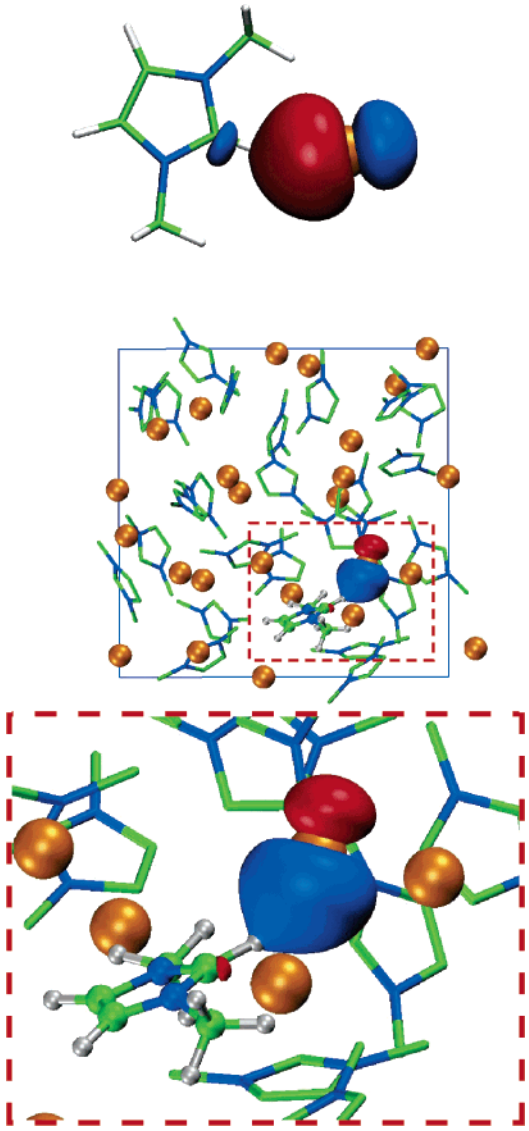

Figure 8. Localized Wannier functions of Cl lone pair orbitals from Car−Parrinello calculations. Top: optimized single ion pair **1**. Middle: snapshot from CPMD simulation in the smaller box. Bottom: enlarged section of the latter.

deserves great care, as these may have a large impact on eventual computational results. Typically, charges are derived from suitable analysis of quantum-mechanical wave functions, usually obtained from static calculations of discrete species in the gas phase. Such an approach has recently been adopted in the design of a force field for ionic liquids.[13] We have now addressed the question how the charge distribution in the dynamic ensemble differs from that in such a discrete monomeric ion pair. To this end, we have obtained Mulliken charges for selected snapshots along the trajectory in the smaller box. The shortcomings of Mulliken population analysis (MPA) are well recognized;[48] to probe its applicability for our purposes, we have computed atomic charges for the isolated ion pair **1** using a variety of theoretical models. From the results summarized in Table 2 it is apparent that the charge distribution within the cation is somewhat sensitive to the actual model or its implementation (for instance, the charge on C^2 can vary between ca. +0.2 and −0.2). The amount of charge transfer, however, as assessed by the charge on Cl, is remarkably similar for all methods. Moreover, the Mulliken charges closely resemble those derived from natural population analysis (NPA) or from fitting to the

electrostatic potential (ESP or ChelpG), which are usually preferable due to reduced basis-set dependence.[48]

The atomic charge on the Cl atom in **1**, which would amount to −1 in the limit of a fully separated ion pair, adopts values between −0.7 and −0.8 with all theoretical models. These values are indicative of substantial charge transfer, fully consistent with the n(Cl) → σ^*(CH) donation discussed above. Most significantly, the CPMD-derived MPA values for static **1** are very similar to the corresponding ensemble averages in the smaller box (compare the last two columns in Table 2). From the standard deviations over all atoms it is also apparent that the overall charge distribution in cations and anions shows only relatively minor instantaneous fluctuations along the trajectory.[49] Thus, the usual procedure to derive force-field atomic charges from data for isolated monomers and to apply these parameters in simulations of bulk ionic liquids appears to be justified.

We note in passing that MPA in CP-opt or CPMD computations is plagued by an incomplete partitioning of the total electron density onto the atomic pseudoorbitals, that is, the corresponding MPA charges in Table 2 do not add up to zero. The total amount of this "unassigned charge" is on the order of ca. 1% of the total number of electrons (i.e., ca. −0.6 per single ion pair),[50] which is most probably contained in regions of a more diffuse density shared by all atoms. The conclusions regarding the fluctuations along the MD trajectory are not affected by this observation.

Dependence on Box Size. The results discussed up to this point were obtained for a rather small periodic box containing just 25 $dmim^+ \cdot Cl^-$ ion pairs. Evidently, more subtle far-order effects cannot be studied with such an approach. To probe for such effects and also for artifacts due to this small box size, we have performed a CPMD simulation for a somewhat larger supercell (comprising 41 ion pairs), which allows extension of the rdfs to about 10 Å. It is in this region, between ca. 8 and 9 Å, where the $g_{ImCl}(r)$ curve derived from the neutron-diffraction data has a shallow maximum, suggesting the presence of a second coordination sphere (see the top of Figure 9). Such a low maximum is also apparent in the CPMD data, albeit shifted to somewhat larger r values (ca. 9−10 Å, see the middle of Figure 9).

It should be kept in mind, however, that due to computational restrictions, we could afford only a short simulation time barely exceeding 2 ps. Certainly no noticeable diffusion or true equilibration can take place on that time scale, and the ion distribution will largely reflect that from the classical MD simulation used to generate the starting configuration. In fact, the Im-Im and Im-Cl rdfs obtained from CPMD and from classical MD (bottom of Figure 9) are remarkably similar, except for the $g_{ImIm}(r)$ curve between 4 and 5 Å, where a local minimum is apparent in the force-field data, as opposed to a couple of local maxima in the CPMD curve. Again, much longer simulation times would be needed in the ab initio dynamics to gauge the significance of this difference.

It is worth noting, however, that the overall near-order in the bulk, as assessed by these rdfs, is quite similar in the CPMD simulations for both supercells (compare the corresponding pictures in Figures 2 and 9). The same is apparent from classical MD runs in periodic boxes of different size (Figure S4). Only minor changes from the rdfs on the bottom of Figure 9 are found when using smaller boxes corresponding in size to those employed in the CPMD simulations.

In particular, the structural pattern in terms of Cl···H interactions is quite comparable among all the simulations, classical or CPMD, performed in this study, and is consistent with similar findings in the literature.[12,13,16] Even though quantitative coordination numbers may change, the principal qualitative feature, namely a strong preference for $C^2-H^2\cdots Cl$ bonding, is not affected by the box size. Thus, the analysis of this interaction discussed above should be generally applicable.

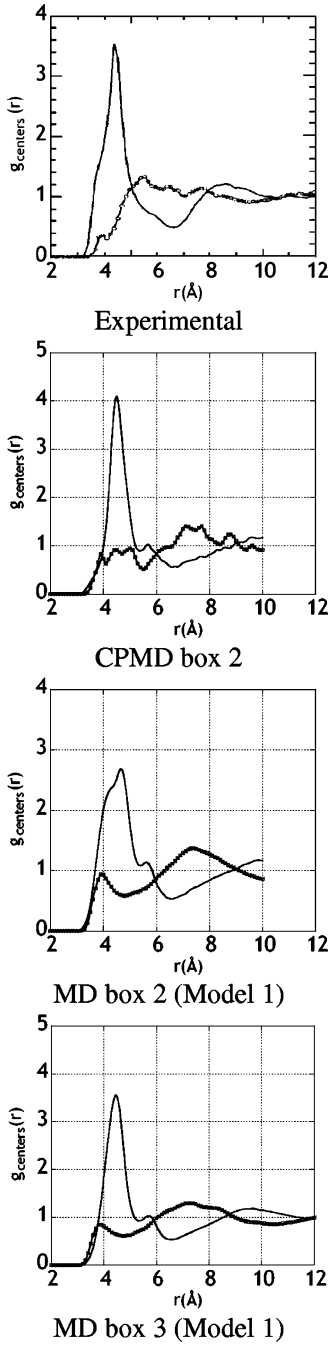

Figure 9. Radial distribution functions for the cation−cation (circle + line) and cation−anion (line) distribution extracted from simulations of larger boxes; from top to bottom: Experimental data derived in ref 16 (reprinted with permission. Copyright 2003, American Institute of Physics). Simulations of 41 ion pairs (box 2), and of 300 ion pairs (box 3). Curves obtained with other AMBER models are given in Supporting Information Figure S5.

The overall insensitivity of these short-range interactions to the box size has also been noted in the other recent DFT-based MD study of Del Pópolo et al. on the same system.[12] They considered a very small box with 8 ion pairs simulated for a total time of about 39 ps (six trajectories of 6−7 ps), and a larger box of 24 ion pairs simulated for 3.5 ps. Despite some inconsistencies concerning structure and energetics of the

isolated monomer,[39] their and our study converge to a similar consensus concerning the directionality of C−H···Cl^- "bonds" in the ionic liquid, which is further supported by our analysis of charge transfer and orbital interactions in the liquid.

Concerning the AMBER simulations of the large box 3 with eight different models, similar qualitative features are also obtained for the Im-Im and Im-Cl rdfs (see Figure S4), as well as for the H-Cl rdfs (Figure S5). All models, including models 6 to 8 with polar $C_{ar}{}^{\delta-}-H^{\delta+}$ bonds fail, however, to account for the directionality of the $C_{ar}-H\cdots Cl^-$ interactions in the liquid (see Figure S6). The distribution of $C_{ar}-H\cdots Cl^-$ angles displays a broad peak around 90° whose intensity (and thus the number of Cl^- ions forming "hydrogen bonds") is quite sensitive to the choice of atomic charges. Extensive optimization and testing of the force field parameters is required, which is beyond the scope of this paper. These preliminary results suggest, however, that in addition to the refinements of force-field parameters for ionic liquids that have been implemented or suggested,[12,13] the treatment of the electrostatics deserves special care.

Conclusion

We have performed extensive CPMD simulations for 1,3-dimethylimidazolium chloride, a prototypical ionic liquid. The microstructure of the liquid has been analyzed in terms of suitable radial distribution functions and anisotropic, site-specific cation−anion distributions. Consistent with previous experience, hydrogen bonding is a guiding motif for rationalizing the near-order present in the liquid. The Cl^- anions show a pronounced preference for positions indicative of CH···Cl bonding, with a particular affinity for the C^2-H^2 site.

We have identified specific orbital interactions that contribute to these preferences. The most important one is charge transfer from a Cl^- lone pair into an antibonding σ^*_{CH} orbital. This donor−acceptor interaction is not only prominent in the static equilibrium structure of the isolated ion pair, but is preserved in the dynamic ensemble of the liquid. According to population analysis of the wave function along the trajectory, the total amount of charge transfer from anions to cations shows only minor instantaneous fluctuations.

Our results confirm and extend related DFT-based simulations on the same system that were being carried out independently. That nonempirical quantum-chemical methods can now be used to study molecular dynamics in ionic liquids is certainly a further step toward a better understanding of structures and properties of this important class of solvents on a molecular level. The short time scale accessible with this kind of MD simulations, however, will remain a challenge for their further application. Far-order phenomena are particularly hard to describe, as they are likely to reflect those in the initial starting configuration. The choice of the latter thus requires great care and, for all practical purposes of their generation, ever more refined classical force fields. On the other hand, near-order phenomena, including the anisotropic cation−anion distribution, are not critically sensitive to the size of the unit cell in periodic calculations. It can thus be anticipated that more complex ionic-liquid systems will be amenable to quantum-chemical simulations in manageably small periodic boxes.

Acknowledgment. M.B. wishes to thank Prof. W. Thiel and the MPI Mülheim for support, the Deutsche Forschungsgemeinschaft for a Heisenberg fellowship, and Prof. Dr. G. Wipff for an invitation to spend a one-month sabbatical in Strasbourg. R.S. thanks the Alexander von Humboldt foundation for a one-month fellowship. Computations were performed on Compaq XP1000 and ES40 workstations at the MPI Mülheim, and on an IBM p690 "Regatta" cluster at the Rechenzentrum Garching of the Max Planck Society.

Supporting Information Available: Two tables detailing the setup of the classical MD simulations, and additional graphical material for analysis of the CPMD trajectories and MD trajectories with different models. This material is available free of charge via the Internet at http://pubs.acs.org.

References and Notes

(1) For selected reviews and monographs see e.g.: (a) Welton, T. *Chem. Rev.* **1999**, *99*, 2071−2083. (b) Rogers, R. D.; Seddon, K. R., Eds. *Ionic Liquids. Industrial applications for Green Chemistry*; ACS Symp. Ser. Vol. 818; American Chemical Society: Washington, DC, 2002.

(2) For selected reviews in organic synthesis see, e.g.: (a) Earle, M. J.; Seddon, K. R. In *Clean Solvents*; Abraham, M. A., Moens, L., Eds.; ACS Symp. Ser. Vol. 819; American Chemical Society: Washington, DC, 2002; pp 10−25. (b) Baudequin, C.; Levillain, J.; Cahard, D.; Gaumont, A. C.; Plaquevent, J. C. *Tetrahedron*: *Asymmetry* **2003**, *14*, 3081−3093. (c) Andrade, C. K. Z.; Alves, L. M. *Curr. Org. Chem*. **2005**, *9*, 195−218.

(3) For selected reviews in catalysis see, e.g.: (a) Gordon, C. M. *Appl. Catal., A* **2001**, *222*, 101−117. (b) Zhao, D. B.; Wu, M.; Kou, Y.; Min, E. *Catal. Today* **2002**, *74*, 157−189. (c) Sheldon, R. A.; Lau, R. M.; Sorgedrager, M. J.; van Rantwijk, F.; Seddon, K. R. *Green Chem*. **2002**, *4*, 147−151. (d) Welton, T. *Coord. Chem. Rev*. **2004**, *248*, 2459−2477. (e) Wasserscheid, P.; Welton, T. *Ionic Liquids in Synthesis*; Wiley-VCH: Weinheim, Germany, 2002.

(4) Arduengo, A. J.; Dias, H. V. R.; Harlow, R. L.; Kline, M. *J. Am. Chem. Soc.* **1992**, *114*, 5530−5534.

(5) Kölle, R.; Dronskowski, R. *Inorg. Chem.* **2004**, *43*, 2803−2809.

(6) Review: Dupont, J. *J. Braz. Chem. Soc*. **2004**, *15*, 341−350.

(7) Turner, E. A.; Pye, C. C.; Singer, R. D. *J. Phys. Chem. A* **2003**, *107*, 2277−2288.

(8) Talaty, E. R.; Raja, S.; Storhaug, V. J.; Dölle, A.; Carper, W. R. *J. Phys. Chem. B* **2004**, *108*, 13177−13184.

(9) For some recent examples see: (a) Urahata, S. M.; Ribeiro, M. C. C. *J. Chem. Phys*. **2005**, *122*, 024511. (b) Del Pópolo, M. G.; Voth, G. A. *J. Phys. Chem. B* **2004**, *108*, 1744−1752. (c) Hanke, C. G.; Lynden-Bell, R. M. *J. Phys. Chem. B* **2003**, *107*, 10873−10878. (d) Margulis, C. J.; Stern, H. A.; Berne, B. J. *J. Phys. Chem. B* **2002**, *106*, 12017−12021. (e) Canongia-Lopes, J. N.; Deschamps, J.; Padua, A. A. H. *J. Phys. Chem. B* **2004**, *108*, 2038−2047. (f) de Andrade, J.; Böes, E. S.; Stassen, H. *J. Phys. Chem. B* **2002**, *106*, 3546−3548.

(10) For instance: (a) Chaumont, A.; Wipff, G. *Inorg. Chem*. **2004**, *43*, 5891−5901. (b) Chaumont, A.; Wipff, G. *Chem. Eur. J.* **2004**, *10*, 3919−3930.

(11) For a semiempirical (AM1) MD study see: Kunsági-Máté, S.; Lemli, B.; Nagy, G.; Kollár, L. *J. Phys. Chem. B* **2004**, *108*, 9246−9250.

(12) For a very recent DFT-based MD study see: Del Pópolo, M. G.; Lynden-Bell, R. M.; Kohanoff, *J. Phys. Chem. B* **2005**, *109*, 5895−5902.

(13) Liu, Z.; Huang, S.; Wang, W. *J. Phys. Chem. B* **2004**, *108*, 12978−12989.

(14) Car, R.; Parrinello, M. *Phys. Rev. Lett*. **1985**, *55*, 2471−2474.

(15) See for instance: Sprik, M. *J. Phys. Condens. Matter* **2000**, *12*, A161−A163 and references therein.

(16) Hardacre, C.; Holbrey, J. D.; McMath, S. E. J.; Bowron, D. T.; Soper, A. K. *J. Chem. Phys*. **2003**, *118*, 273−278.

(17) Empirical potential structure refinement process: (a) Soper, A. K. *Chem. Phys*. **1996**, *202*, 295−306. (b) Soper, A. K. *Mol. Phys*. **2001**, *99*, 1503−1516.

(18) (a) Hehre, W. J.; Ditchfield, R.; Pople, J. A. *J. Chem. Phys.* **1972**, *56*, 2257−2261. (b) Hariharan, P. C.; Pople, J. A. *Theor. Chim. Acta* **1973**, *28*, 213−222. (c) Clark, T.; Chandrasekhar, J.; Spitznagel, G. W.; Schleyer, P. v. R. *J. Comput. Chem.* **1983**, *4*, 294−301.

(19) Becke, A. D. *Phys. Rev. A* **1988**, *38*, 3098−3100.

(20) Perdew, J. P. *Phys. Rev. B* **1986**, *33*, 8822−8824. Perdew, J. P. *Phys. Rev. B* **1986**,*34*, 7406.

(21) Lee, C.; Yang, W.; Parr, R. G. *Phys. Rev. B* **1988**, *37*, 785−789.

(22) (a) Perdew, J. P.; Burke, K.; Ernzerhof, M. *Phys. Rev. Lett*. **1996**, *77*, 3865−3868. (b) Perdew, J. P.; Burke, K.; Ernzerhof, M. *Phys. Rev. Lett*. **1997**, *78*, 1396.

(23) Becke, A. D. *J. Chem. Phys.* **1993**, *98*, 5648−6552.

(24) Frisch, M. J.; Trucks, G. W.; Schlegel, H. B.; et al. *Gaussian 98*; Gaussian, Inc.: Pittsburgh, PA, 1998.

(25) Frisch, M. J.; Trucks, G. W.; Schlegel, H. B.; et al. *Gaussian 03*; Gaussian, Inc.: Pittsburgh, PA, 2003.

(26) *CPMD* Version 3.7.0.; Copyright by IBM Corp. and Max-Planck-Institut für Festkörperforschung: Stuttgart, Germany.

(27) Troullier, N.; Martins, J. L. *Phys. Rev. B* **1991**, *43*, 1993−2006.

(28) Kleinman, L.; Bylander, D. M. *Phys. Rev. Lett.* **1982**, *48*, 1425−1428.

(29) Reed, A. E.; Curtiss, L. A.; Weinhold, F. *Chem. Rev.* **1988**, *88*, 899−926.

(30) (a) Singh, U. C.; Kollman, P. A. *J. Comput. Chem.* **1984**, *5*, 129−145. (b) Besler, B. H.; Merz, K. M., Jr.; Kollman, P. A. *J. Comput. Chem.* **1990**, *11*, 431−439.

(31) Breneman, C. M.; Wiberg, K. B. *J. Comput. Chem.* **1990**, *11*, 361−373.

(32) Atomic orbitals were taken from the pseudo wave functions involved in construction of the pseudopotentials, except for hydrogen, where a standard Slater function was used.

(33) (a) Wannier, G. H. *Phys. Rev.* **1937**, *52*, 191−197. (b) Berghold, G.; Mundy, C. J.; Romero, A. H.; Hutter, J.; Parrinello, M. *Phys. Rev. B* **2000**, *61*, 10040−10048.

(34) Case, D. A.; Pearlman, D. A.; Caldwell, J. W.; Cheatham, T. E., III; Wang, J.; Ross, W. S.; Simmerling, C. L.; Darden, T. A.; Merz, K. M.; Stanton, R. V.; Cheng, A. L.; Vincent, J. J.; Crowley, M.; Tsui, V.; Gohlke, H.; Radmer, R. J.; Duan, Y.; Pitera, J.; Massova, I.; Seibel, G. L.; Singh, U. C.; Weiner, P. K.; Kollman, P. A. *AMBER7*; University of California: San Francisco, *CA*, 2002.

(35) de Andrade, J.; Böes, E. S.; Stassen, H. *J. Phys. Chem. B* **2002**, *106*, 13344−13351.

(36) Morrow, T. I.; Maginn, E. J. *J. Phys. Chem. B* **2002**, *106*, 12807−12813.

(37) Hanke, C. G.; Price, S. L.; Lynden-Bell, R. M. *Mol. Phys.* **2001**, *99*, 801−809.

(38) By 1.5 kcal/mol with dielectric constants of 10 and 78, as obtained from single point calculations using the Polarizable Continuum Model (Barone, V.; Cossi, M.; Tomasi, J. *J. Comput. Chem.* **1998**, *19*, 404. Cossi, M.; Scalmani, G.; Rega, N.; Barone, V. *J. Chem. Phys.* **2002**, *117*, 43. Cossi, M.; Crescenzi, O. *J. Chem. Phys.* **2003**, *19*, 8863) as implemented in Gaussian 03.

(39) However, the PBE-optimized parameters reported with the procedure adopted in ref 12 (**1**: $r_1 = 1.74$ Å, $r_3 = 1.2$ Å; **2**: $r_1 = 2.20$ Å) differ conspicuously from our PBE/6-31+G** data in Table 1, which could be indicative of an overestimation of the cation−anion interaction with the former approach. Also, Del Pópolo et al. find that perpendicular π-coordinated **2** is preferred over in-plane coordinated **1** (by 3.2 kcal/mol), whereas we find the opposite result at all DFT levels including PBE (Table 1). In any event, the two forms are close in energy, and mimicking the solvent by an empirical solvation model is sufficient to enhance the preference for in-plane coordination, as found in the solid-state structure and in the liquid state.

(40) Fannin, A. A., Jr.; Florcani, D. A.; King. L. A.; Landers, J. S.; Piersma, B. J.; Stech, D. J.; Vaughn, R. L.; Wilkes, J. S.; Williams, J. L. *J. Phys. Chem.* **1984**, *88*, 2614−2621.

(41) For the definition of the pair correlation function see, for example: Allen, M. P.; Tildesley, D. J. *Computer Simulation of Liquids*; Clarendon Press: Oxford, UK, 1987.

(42) The performance of AMBER to describe geometries and interaction energies of stacked N-heterocyclic aromatics (such as DNA base pairs) is usually quite good, but can depend on the particular system, see, e.g.: (a) Hobza, P.; Kabeláč, M.; Šponer, J.; Mejzlík, P.; Vondrá×f0ek, J. *J. Comput. Chem.* **1997**, *18*, 1136−1150. (b) Řeha, D.; Kabeláč, M.; Ryáček, F.; Šponer, J.; Šponer, J. E.; Elstner, M.; Suhai, S.; Hobza, P. *J. Am. Chem. Soc.* **2002**, *124*, 3366−3376.

(43) Shim, Y.; Duan, J.; Choi, M. Y.; Kim, H. Y. *J. Phys. Chem.* **2003**, *119*, 6411−6414.

(44) Yan, T.; Burnham, C. J.; Del Pópolo, M. G.; Voth, G. A. *J. Phys. Chem. B* **2004**, *108*, 11877−11881

(45) For recent monographs and reviews, see, e.g.: (a) Desiraju, G. R.; Steiner, T.; *The Weak Hydrogen Bond in Structural Chemistry and Biology*; Oxford University Press: Oxford, UK, 1999. (b) Steiner, T. *Angew. Chem., Int. Ed.* **2002**, *41*, 48−76. (c) Meot-Ner (Mautner), M. *Chem. Rev.* **2005**, *105*, 213−284.

(46) Wiberg, K. *Tetrahedron* **1968**, *24*, 1083−1096.

(47) For instance: (a) Guerra, C. F.; Bickelhaupt, F. M.; Snijders, J. G.; Baerends, E. J. *Chem. Eur. J.* **1999**, *5*, 3581−3594. (b) Bühl, M.; Wipff, G. *J. Am. Chem. Soc.* **2002**, *124*, 4473−4480. (c) Kryachko, E. S.; Zeegers-Huyskens, T. *J. Phys. Chem. A* **2002**, *106*, 6832−6838.

(48) Wiberg, K. B.; Rablen, P. R. *J. Comput. Chem.* **1993**, *14*, 1504−1518.

(49) The significance of this bonding analysis should be unaffected by possible incomplete equilibration of the cation−cation distribution, see above.

(50) Similar values for the unassigned charge were found in CPMD results for an ionic solid: Haiber, M.; Ballone, P.; Parrinello, M. *Am. Mineral.* **1997**, *82*, 913−922.